Electronic Supplementary Material (ESI) for Dalton Transactions.

Supporting information for

3D Ni and Co Redox-Active Metal-Organic Frameworks Based on Ferrocenyl Diphosphinate and 4,4'-Bipyridine Ligands as Efficient Electrocatalysts for Hydrogen Evolution Reaction

Vera Khrizanforova, Ruslan Shekurov, Vasily Miluykov, Mikhail Khrizanforov, Volodymyr Bon, Stefan Kaskel, Aidar Gubaidullin, Oleg Sinyashin and Yulia Budnikova

1. Synthesis of starting materials, and coordination polymers 1 - 4

Reagent 1,1'-ferrocenylenbis(*H*-phosphinic) acid (**H_2fcd*H*p**) was prepared according to the literature procedure.[1] Coordination polymers $[M(bpy)]_n$ (M=Ni, Co) **3** and **4** was prepared according to the literature procedure [2]. All other chemicals and solvents were purchased reagent grade and used as received.

Synthesis of poly-((μ2-4,4'-bipyridyl-N,N′)-bis(μ2-1,1'-ferrocenyl-bis(H-phosphinate)nickel (II)) **Nibpyfcd*H*p** (**1**). $Ni(NO_3)_2 \cdot 6H_2O$ (47 mg, 0.16 mmol), 4,4'-bipyridine (25 mg, 0.16 mmol) in 4 ml DMF/MeOH (1:1) solution was added to 50 mg (0.16 mmol) H_2fcd*H*p dissolved in DMF/MeOH (1:3 v/v, 4 mL). The resulting mixture was heated for 12 hours at 80 ° C, a part of the methanol was evaporated and the orange crystals of compound **1** was formed with yield of 0.077 g (86%). Orange crystals were dried in air. Anal. calcd. for $C_{21}H_{22}N_2FeNiO_5P_2$ (558.90): C, 45.09; H, 3.94. Found: C, 44.83; H, 3.99.

IR (KBr, cm^{-1}): 3580 (m), 3423 (m), 3116 (m), 3093 (m), 3075 (m), 2930 (m), 2370 (m), 1603 (m), 1482 (m), 1412 (m), 1218 (m), 1178 (s), 1061 (s), 1020 (s), 970 (s), 832 (m), 647 (m), 635 (m), 558 (w), 528 (m), 474 (s).

Synthesis of **Cobpyfcd*H*p** (**2**). The identical reaction conditions except for the use of $Co(NO_3)_2 \cdot 6H_2O$ (25 mg, 0.16 mmol) instead of $Ni(NO_3)_2 \cdot 6H_2O$ were employed to produce dark orange crystals of **2**. Yield: 57%. Anal. $C_{21}H_{22}N_2FeCoO_5P_2$ (559.14): 45.07; H, 3.93. Found: C, 45.07; H, 3.84

IR (KBr, cm^{-1}): 3583 (m), 3423 (m), 3093 (m), 3075 (m), 2927 (w), 2373 (m), 1601 (m), 1481 (m), 1412 (m), 1217 (w), 1175 (s), 1059 (s), 1049 (s), 970 (s), 831 (m), 647 (m), 629 (m), 527 (m), 502 (m), 472 (s).

2. Structure determination

The dataset from the single crystal of **1**, prepared in a nylon cryoloop and "Paratone-N" oil, was collected at beamline BL14.2, Joint Berlin-MX Laboratory of Helmholtz Zentrum Berlin, equipped with a MX-225 CCD detector (Rayonics, Illinois) and 1-circle goniometer.[3] The data collection was performed at 263 K using X-ray radiation with $\lambda = 0.88561$ Å. XDSAPP 2.0 software was used for processing of the diffraction images.[4] The structure was solved by direct methods and refined in anisotropic approximation for all non-H atoms by least-square on F^2 using SHELX 2016/4 software.[5] Hydrogen atoms connected to carbons were placed in geometrically calculated positions and refined using "riding model" with $U_{iso}H = 1.5U_{iso}C$ for CH_3 and $U_{iso}H = 1.2U_{iso}C$ for all other atoms. Hydrogen atoms on phosphinic group and methanol oxygen were found from the difference Fourier map and refined freely. Distance restraint of 0.86 Å was applied to methanol O-H group in order to keep the bond length within the chemically reasonable value. Methyl group of the lattice methanol is disordered over two positions related by two-fold rotation axis and refined with occupancy of 0.5.

CCDC 1970682 contains the supplementary crystallographic data for this paper. These data can be obtained free of charge from the Cambridge Crystallographic Data Centre via www.ccdc.cam.ac.uk/data_request/cif.

1: $C_{21}H_{22}FeN_2NiO_5P_2$, M = 558.90 g/mol, crystal size (mm) 0.08x0.05x0.05, temperature 263(2) K, orthorhombic, space group *Pnna* (No. 52), a = 10.710(2), b = 17.590(4), c = 11.290(2) Å, V = 2126.9(7) Å^3, Z = 4, ρ_{calc} = 1.745 g·cm^{-3}, μ = 3.193 mm^{-1}, θ range: from 2.89° to 32.10°, 16045 reflection collected (*-13 ≤ h ≤ 13, -22 ≤ k ≤ 22, -14 ≤ l ≤ 14*), 2354 independent reflections (R_{int} = 0.057), 2036 observed reflections with $I \geq 2\sigma(I)$, 156 refined parameters, R = 0.043, wR^2 = 0.108, max. residual electron density 1.154 (-0.722) eÅ^{-3}.

Table S1. Selected bon lengths and angles for 1.

Bond	D, Å	Angle	°
Ni(1) – O(2)	2.075(2)	O(2) - Ni(1) - O(1)	88.50(8)
Ni(1) – O(1)	2.077(2)	O(2) - Ni(1) - O(1)	91.49(8)
Ni(1) – N(1)	2.096(3)	O(1) - Ni(1) -N(1)	89.91(6)
Ni(1) – N(2)	2.113(4)	O(2) - Ni(1) - N(1)	86.63(6)
		O(2) - Ni(1) - N(2)	93.37(6)
		O(1) - Ni(1) - N(2)	90.09(6)

3. Magnetic properties of 1 and 2

We investigated magnetic properties of **1** and **2** complexes. The g-values of complexes are obtained from ESR measurement at room temperature at frequency 9.56 GHz. The static magnetization M of the samples were measured on powder samples in the temperature range T = 1.8-300 K and in magnetic fields μ_0H up to 7T. Their magnetic susceptibility as function of temperature are simulated by the Curie-Weiss law $\chi=C/(T+\theta)+\chi_0$, where C is the Curie constant, θ is the Curie-Weiss temperature, and χ_0 is temperature independent diamagnetic contribution. From the Curie constant, the value of the effective magnetic moment μ_{eff} per molecule was calculated which can be expressed as $\mu_{eff}=g[s(s+1)]^{1/2}$. This equation was used to calculate the effective spin of formula unit (F.U.). The magnetic behavior and the strength of the magnetic interaction are indicated from sing and magnitude of the Curie-Weiss temperature, respectively. A saturation magnetization observed from the field dependence of the magnetization M(H) gives a total spin per formula unit.

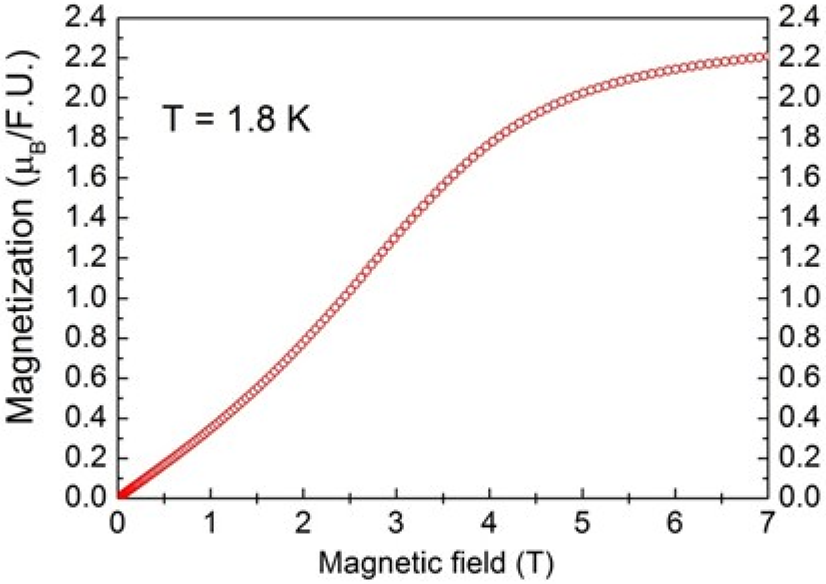

Figure S1. Field dependence of the magnetization M(H) of the **2** complex at T = 1.8 K.

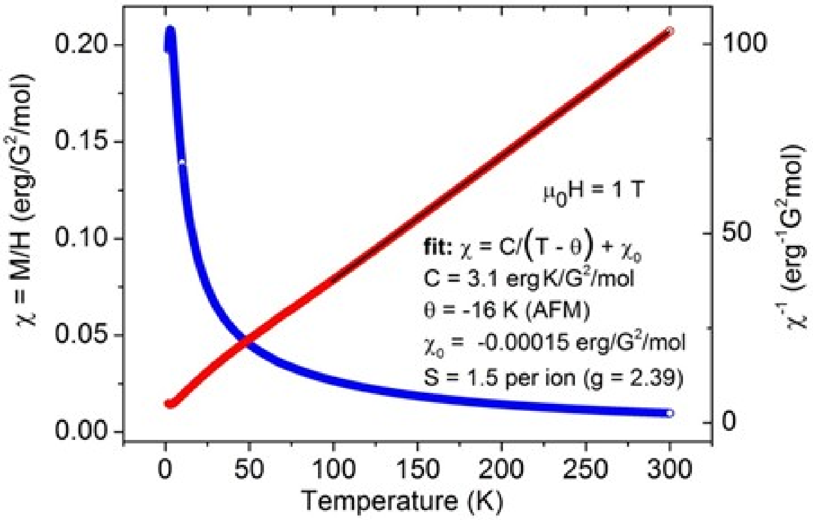

Figure S2 Temperature dependence of the static magnetic susceptibility $\chi_m = M/H$ of **2** and the corresponding inverse susceptibility χ_m^{-1} with the Curie-Weiss model.

The field dependence of the magnetization M(H) at 1.8 K is presented in Fig. 1. These measurements reveals the magnetization is not saturated at μ_0H=7T. The shape of the magnetization is not fit with brillouin function like paramagnetic species. This characteristic change of the slope of the magnetization versus magnetic field M(H) indicates antiferromagnetic interaction between Co(II) ions in neighboring formula units.

For Temperature dependence of the static magnetic susceptibility, the fit yields the Curie-Weiss temperature of -16K which indicates an antiferromagnetic coupling between Co(II) ions in neighboring formula unit, a temperature independent diamagnetic component χ_0 =-0.00015 erg/G^2/mole, and C=3.1 erg/G^2/mole. From the Curie-Weiss constant, S_{eff}=1.5 per molecule was calculated.

1:

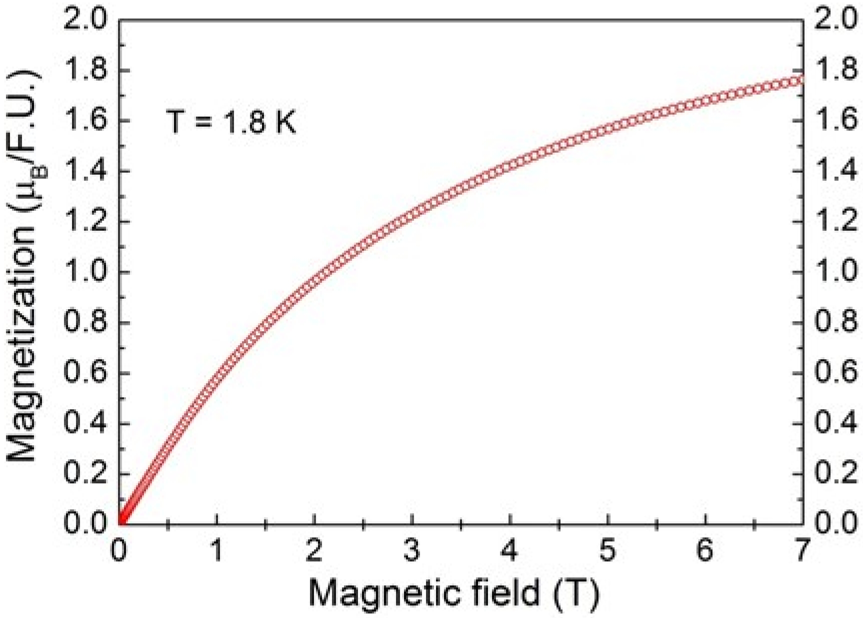

Figure S3. Field dependence of the magnetization M(H) of the **1** complex at T = 1.8 K.

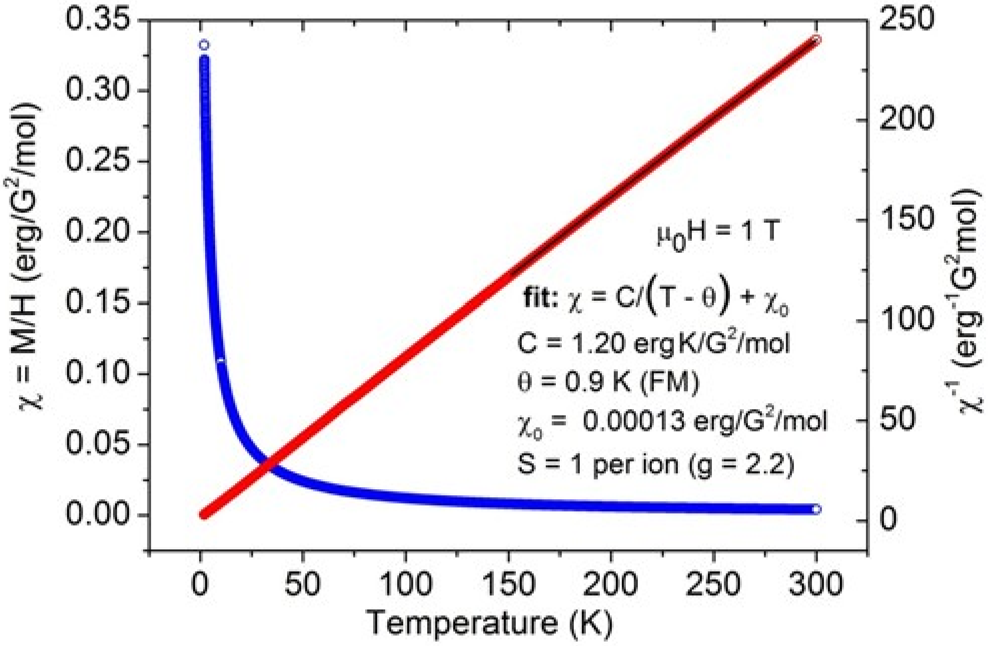

Figure S4. Temperature dependence of the static magnetic susceptibility χ_m = *M*/*H* of **1** and the corresponding inverse susceptibility χ_m^{-1} with the Curie-Weiss model.

The field dependence of the magnetization M(H) at 1.8 K is presented in Fig. 3. These measurements reveals the magnetization is not saturated at μ_0H=7T.

For temperature dependence of the static magnetic susceptibility, the observed Curie-Weiss temperature of 0.9K is too small and can be considered as an error bar in simulation. It indicates there is no interaction between Ni(II) ions in neighboring formula unit. The fit yields a temperature independent diamagnetic component χ_0 =-0.00013 erg/G²/mole, and C=1.2 erg/G²/mole. From the Curie-Weiss constant, S_{eff}=1 per molecule was calculated.

4. *Electrochemical data*

Electrochemical measurements were taken on a BASiEpsilonE2P electrochemical analyzer (USA). The program concerned Epsilon-EC-USB-V200 waves. A conventional three-electrode system was used with glassy carbon electrode modified with MOF Nafion coated for powder samples as the working electrode, the Fc^+/Fc system or RHE were served as reference electrodes, and a Pt wire as the counter electrode. 0.1 M Et_4NBF_4 was used as the supporting electrolyte to determine the current–voltage characteristics. The performances of electrocatalysts can be evaluated by many parameters, such as the onset potential overpotential (η) at a specific current density (j=10 mA cm^{-2}), Tafel slope (TS), turnover frequency (TOF), stability/durability.
Supposing that all the current is used for the electrochemical reaction, the theoretical TOF value in 0.5 M H_2SO_4 can be simply calculated by $TOF_{theoretical} = j/(n \times F \times m/M)$ [6] where n is the number of electrons involved in reaction, m is the mass loading of the catalyst (mg cm–2), and M is the molecular weight of the catalyst unified with one active center per formula unit.

The turnover frequencies in CH_3CN using $[(DMF)H]^+$ as acid were determined using equation:

$$\text{TOF} = \upsilon \cdot \left(\frac{i_{cat}/i_p}{0.72} \right)^2$$

from i_{cat}/i_p values [7]. i_{cat} is the catalytic current measured in the presence of acid, i_p is the peak current in the absence of acid for MOF, v is scan rate in V/s.

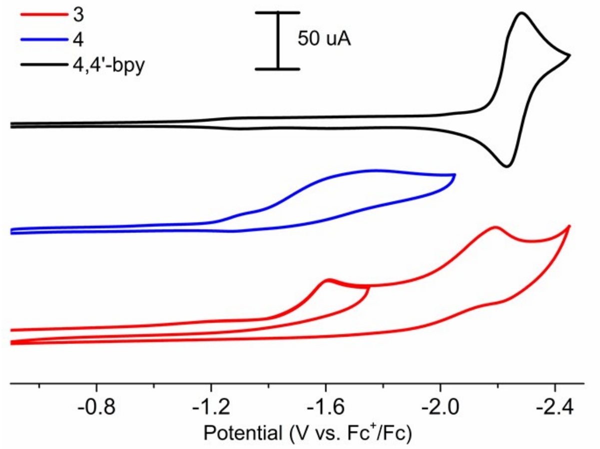

Figure S5 CVs of 4,4'-bpy, polymers **3** and **4** in MeCN/Bu_4NBF_4. Conditions: Glassy carbon electrode(GCE)/MOF/Nafion.

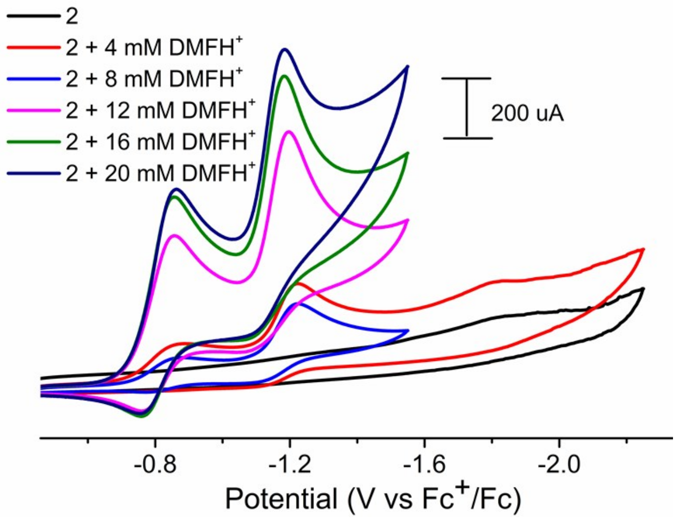

Figure S6 CVs for **2** in MeCN/Bu_4NBF_4 in the presence of increasing amounts DMFH$^+$. Conditions: GCE/MOF/Nafion.

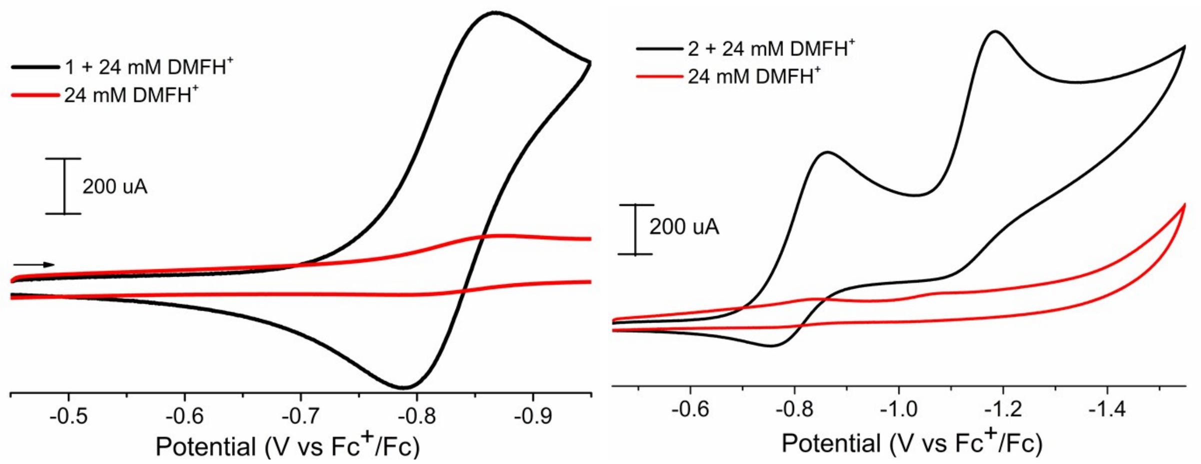

Figure S7 CVs for **1** (left) and **2** (right) with 24 mM DMFH$^+$ in 0.1 M Bu_4NBF_4 in MeCN. Conditions GCE/MOF (**1** or **2)** /Nafion (black) and bare GCE.

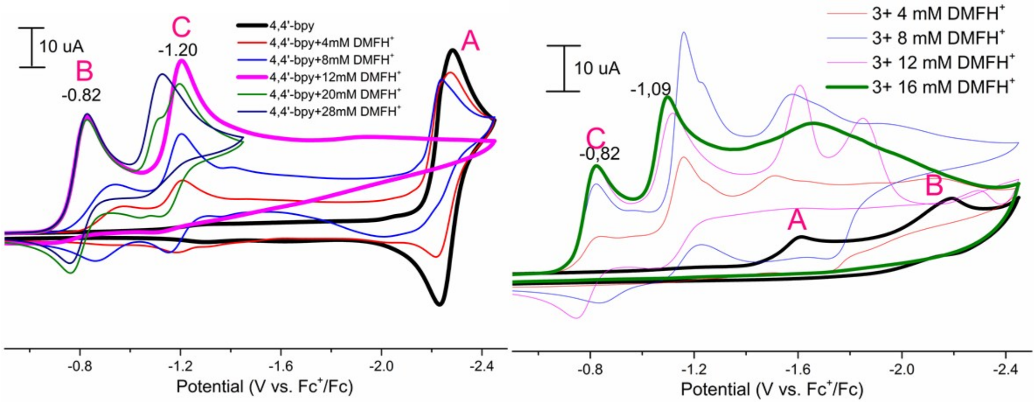

Figure S8 (left) CVs of 5mM solution of 4.4'-bpy on GC working electrode and (right) **3** (GCE/MOF/Nafion) in the presence of increasing amounts of $DMFH^+$ in 0.1 M Bu_4NBF_4 in MeCN

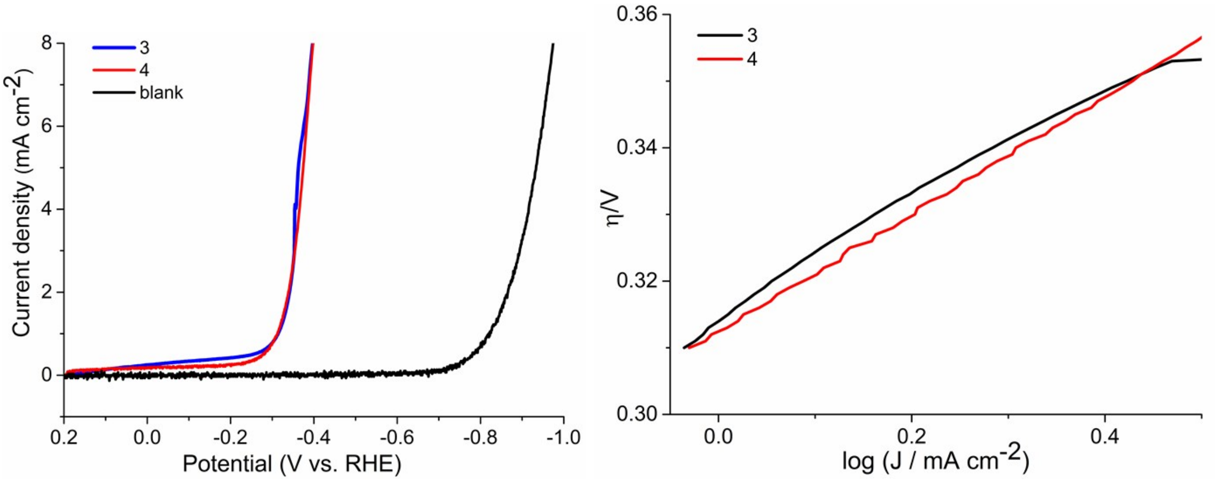

Figure S9 Electrochemical characterization of the prepared catalysts: LCV polarization curves obtained for **3** and **4** in 0.5 M H_2SO_4 at 0.05 V/s and the corresponding Tafel plots.

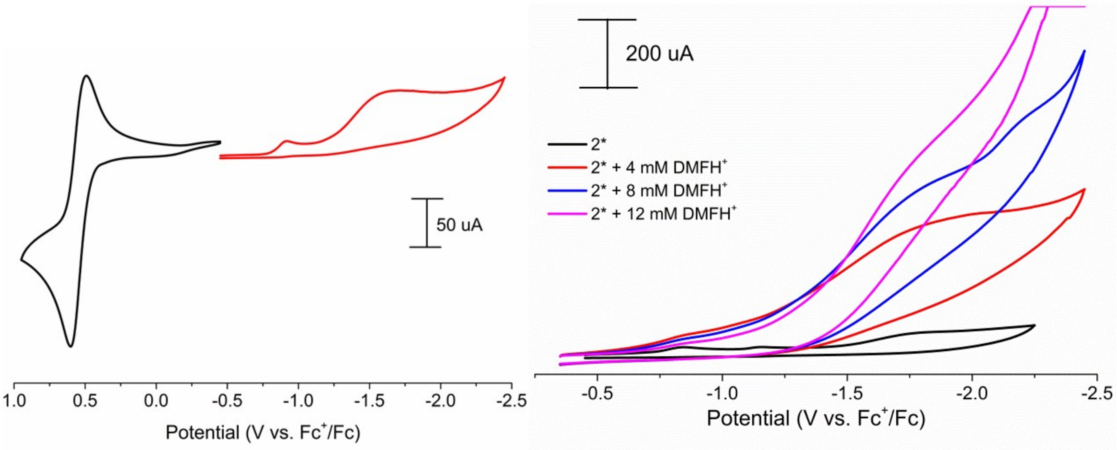

Figure S10 CVs of **2*** (polymer **2** after 1 day in 0,5 M H_2SO_4) (left) in MeCN/Bu_4NBF_4. (right) CVs for **2*** in MeCN/Bu_4NBF_4 in presence of $DMFH^+$. Conditions: GCE/MOF/Nafion

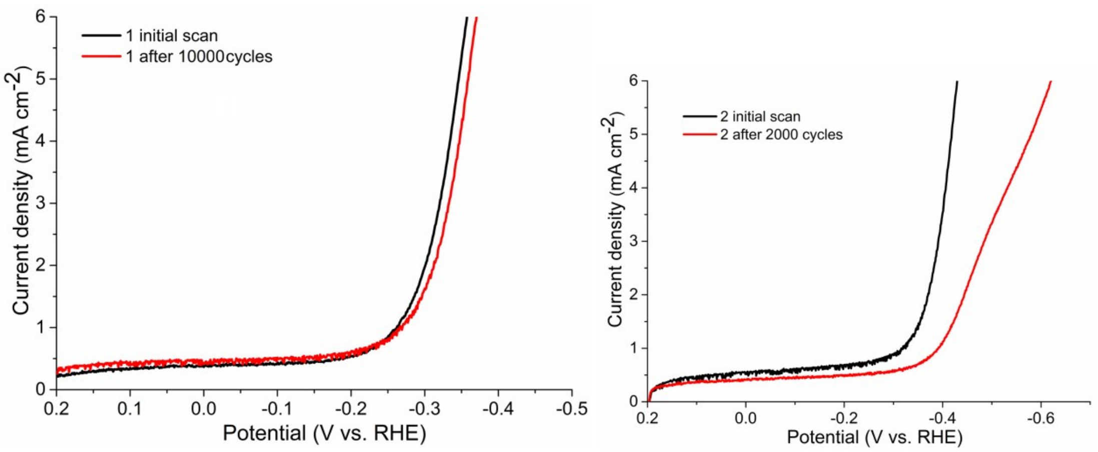

Figure S11 LSVs for **1** (left) and **2** (right) before and after 10,000 (for **1**) or 2000 (for **2**) CV scans in 0.5M H_2SO_4. Conditions: GCE/MOF/Nafion

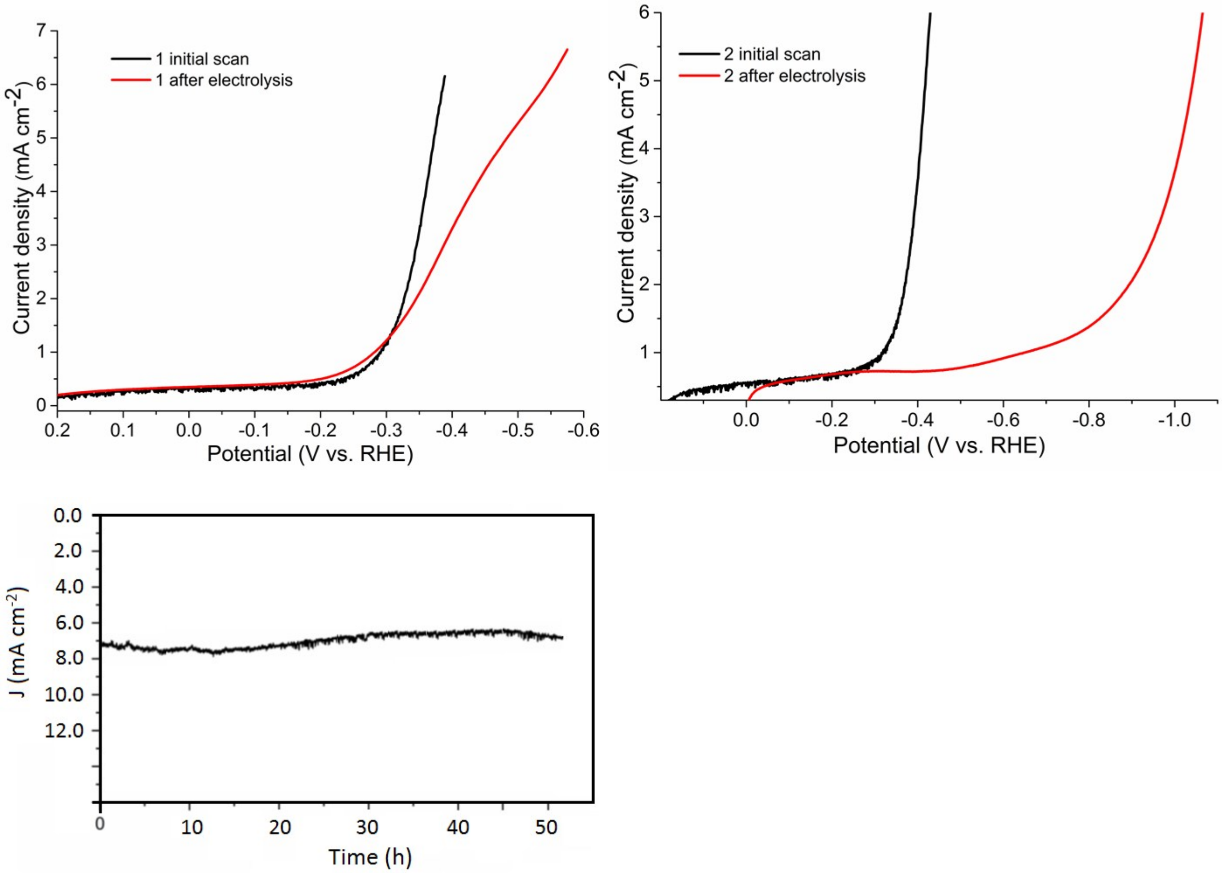

Figure S12 LSVs for **1** (left) and **2** (right) after 30 hours of controlled potential electrolysis at 400 mV vs the RHE in 0.5M H_2SO_4 . Below: Chronopotentiometric curve of the **1** modified electrode at a constant current density of 7 mAcm^{-2}.

5. *Powder X-ray diffraction*

The X-ray diffraction analysis was performed on the equipment of Spectral-Analytical Center of FRC Kazan Scientific Center of RAS. Powder X-ray diffraction (PXRD) measurements were performed on a Bruker D8 Advance diffractometer equipped with Vario attachment and Vantec linear PSD, using Cu radiation (40 kV, 40 mA) monochromated by the curved Johansson monochromator (λ Cu $K_{\alpha1}$ 1.5406 Å). Room-temperature data were collected in the reflection mode. The samples were loaded on a standard zero diffraction silicon plate, which was kept spinning (15 rpm) throughout the data collection. Patterns were recorded in the 2Θ range between 3° and 90°, in 0.008° steps, with a step time of 0.1–1.0s. *For each sample several experiments were performed, allowing to control stability of the samples and quality of the experiments.* Processing of the obtained data performed using EVA [DIFFRAC Plus Evaluation package EVA, Version 11 (2005). User's Manual, Bruker AXS, Karlsruhe. Germany. - 258 p] software packages.

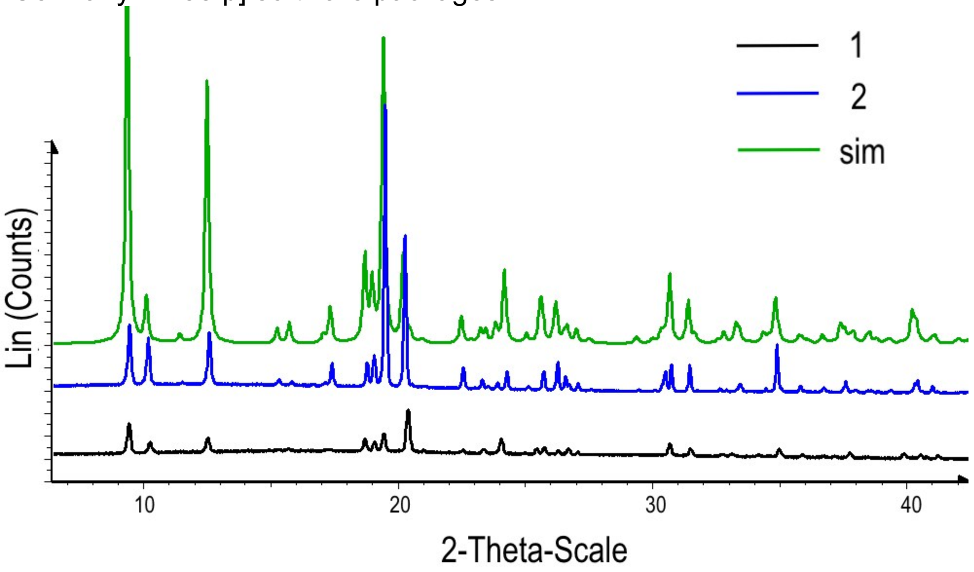

Figure S13 Experimental and simulated PXRD data for **1** and **2**

A comparison of the experimental diffractograms of polymers **3** and **4** with the theoretical simulated diffractogram (Figure S14), calculated according to single crystal X-ray diffraction analysis of a crystal $\{[Co_2(4,4'\text{-bpy})_3(NO_3)_4]$ 'X $H_2O\}_n$,, indicates a significant difference the crystalline structure of polymers **3** and **4** from the structure of the 3D polymer described in [2]. The crystal structure of the Co complex was established in this work, but the authors also report the isostructural nature of the complexes with Co, Ni, and Zn and refer to the data of powder diffraction. Unfortunately, the data of powder diffraction in the article and in additional materials are not available, which did not allow a direct comparison of the data of powder diffraction of these polymers.

In the case of the Ni- and Co complexes **3** and **4** that we obtained, a significant similarity between their experimental diffraction patterns can be noted, especially in the initial part of them, in which reflections from the basal planes of the crystal cell are usually located. This, in turn, indicates close values of the unit cell parameters of these polymers, but does not exclude the possibility of their crystallization with water molecules in various stoichiometric ratios.

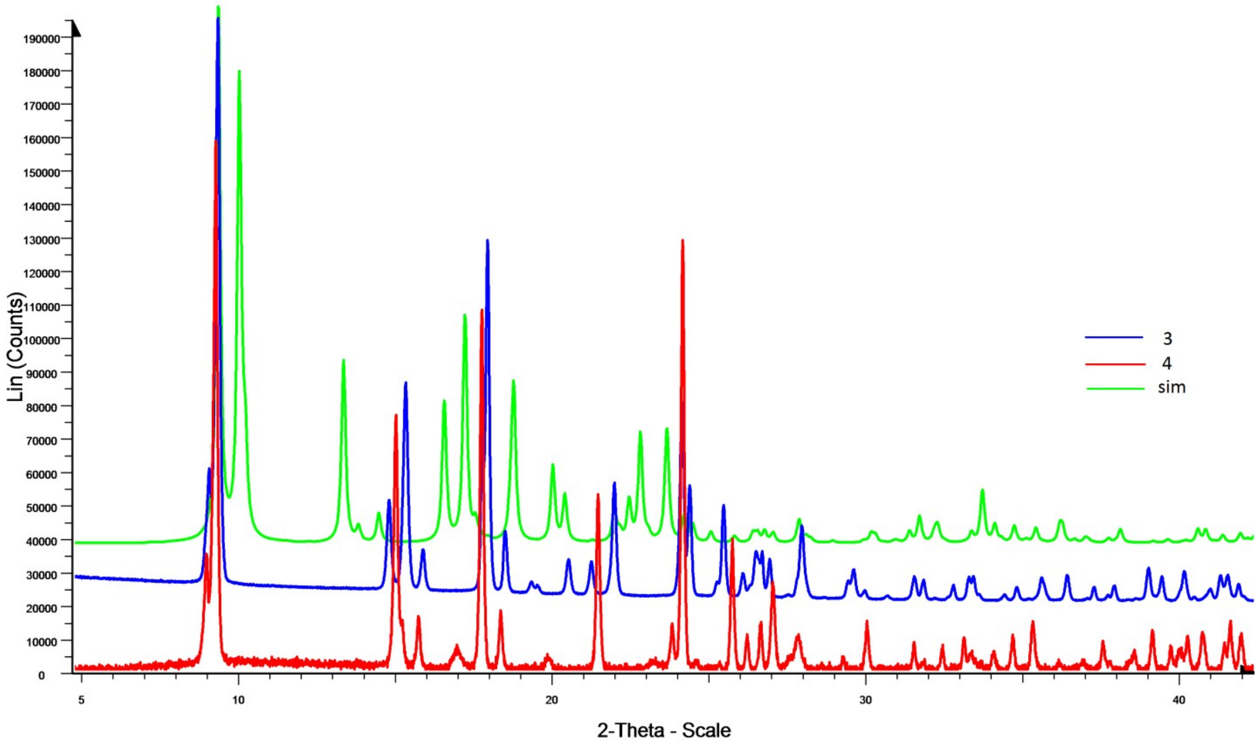

Figure S14 Experimental PXRD data for **3** (blue) and **4** (red) and simulated for complex $\{[Co_2(4,4'\text{-}bpy)_3(NO_3)_4]\cdot xH_2O\}_n$ (green) (in accordance with single crystal data in [2]).

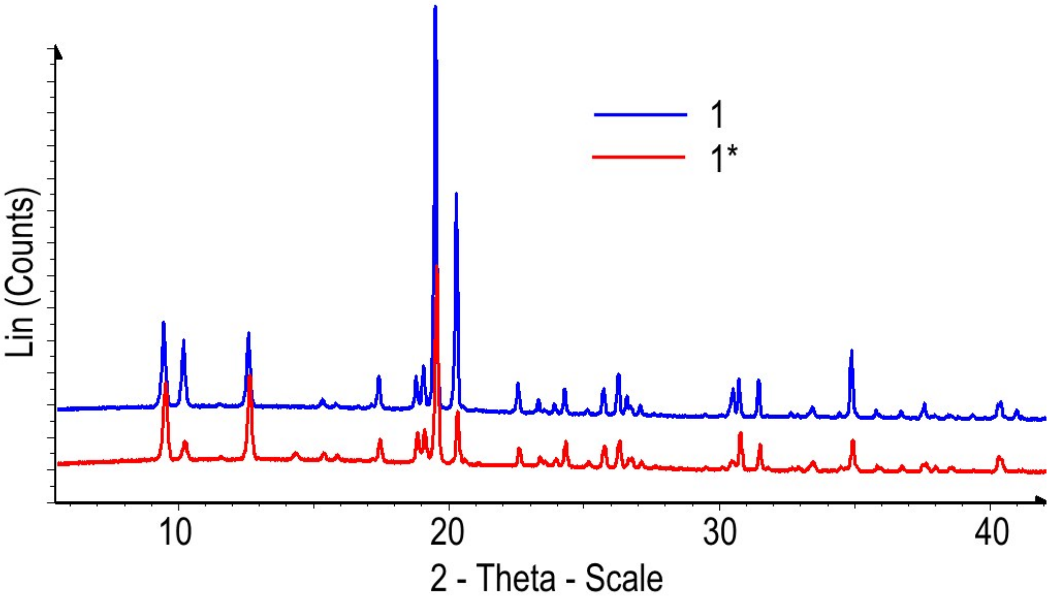

Figure S15 Experimental PXRD data for samples **1** and **1***

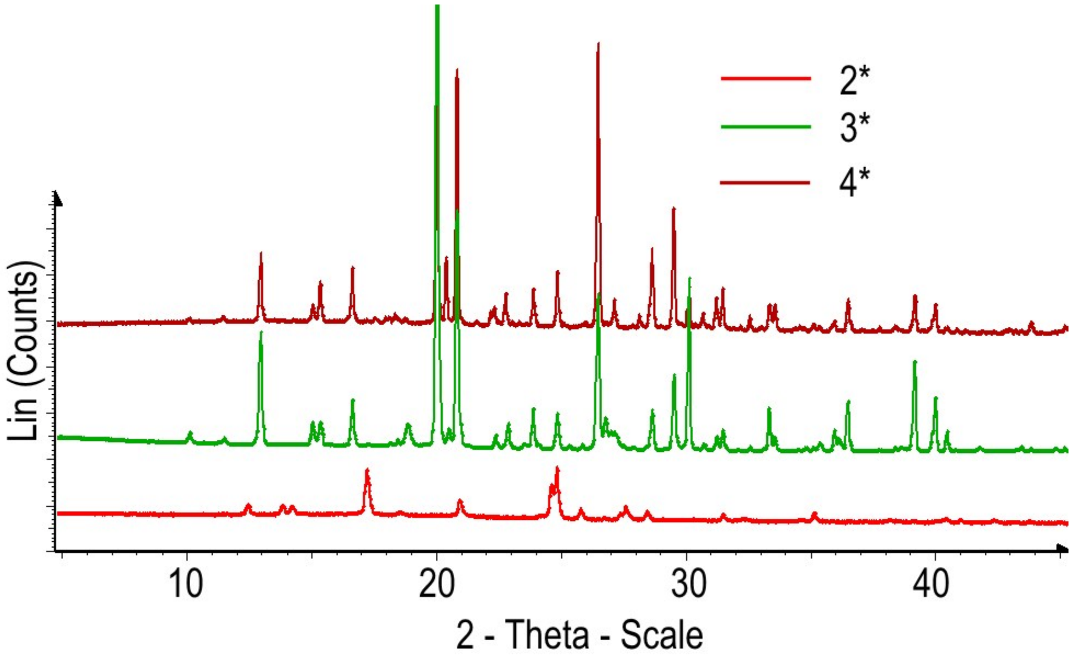

Figure S16 Experimental PXRD data for samples **2***, **3*** and **4***

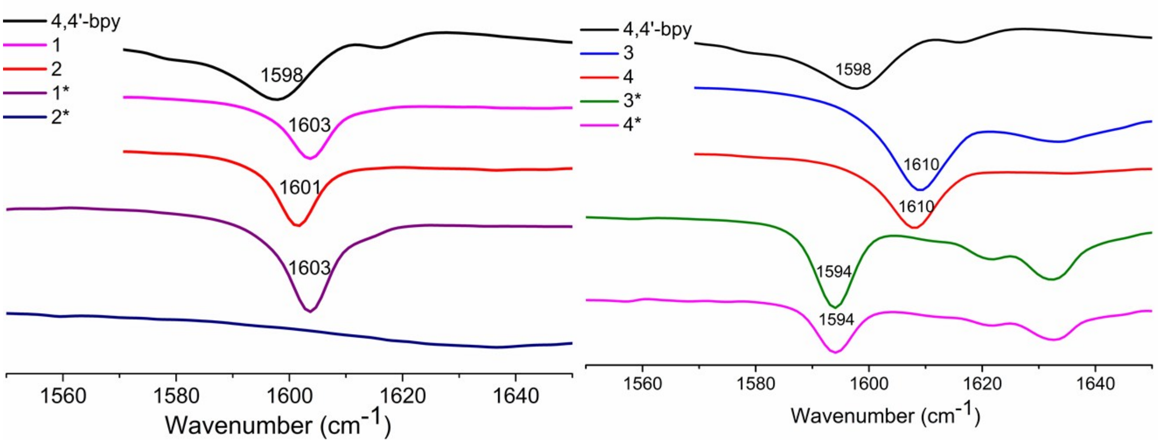

Figure S17 IR spectra for **1** – **4** and **1*** - **4***

6. Elemental analysis for 3D Ni and Co Redox-Active Metal-Organic Frameworks Based on Ferrocenyl Diphosphinate and 4,4'-Bipyridine Ligands 1 and 2 based on X-ray fluorescence data and EDS data

X-ray fluorescence spectra were obtained using an energy-dispersive X-ray spectrometer EDX 800HS2 (Shimadzu). It has an active diameter of 10 mm. All measurements were made using a 50 W low-power Rh tube (50 kV) with an acquisition time of 100 s (live time).

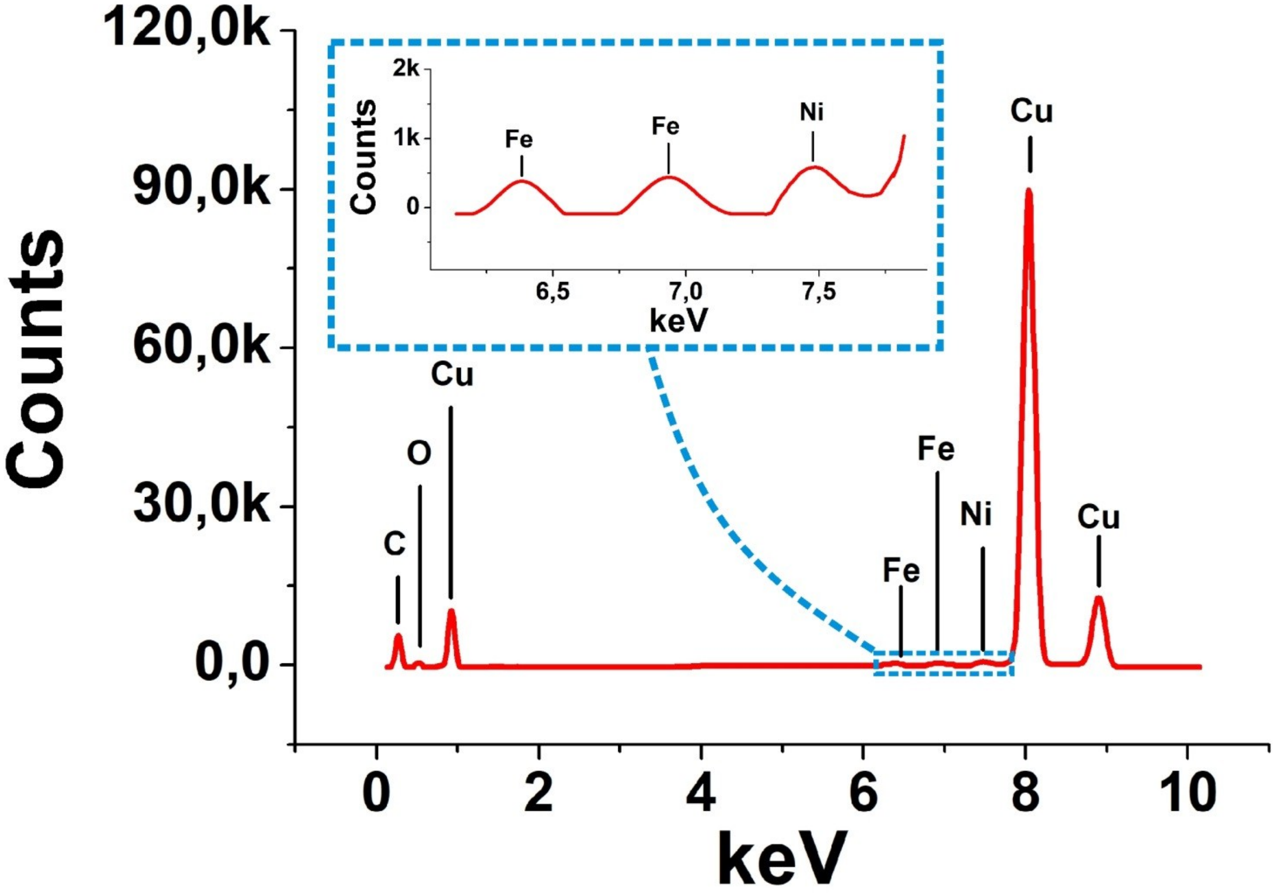

Figure S18 EDS spectrum of **1**. In the spectrum, against the background of intense copper lines, the nickel line $K_{\alpha 1}$ = 7.48 keV is visible. In addition to the nickel line, the spectrum contains iron lines ($K_{\alpha 1}$ = 6.41 keV, $L_{\beta 1}$ = 7.06 keV), carbon line ($K_{\alpha 1}$ = 0.28 keV), oxygen line ($K_{\alpha 1}$ = 0.53 keV) and copper lines ($L_{\alpha 1}$ = 0.93 keV, $K_{\alpha 1}$ = 8.05 keV, $K_{\beta 1}$ = 8.90 keV).

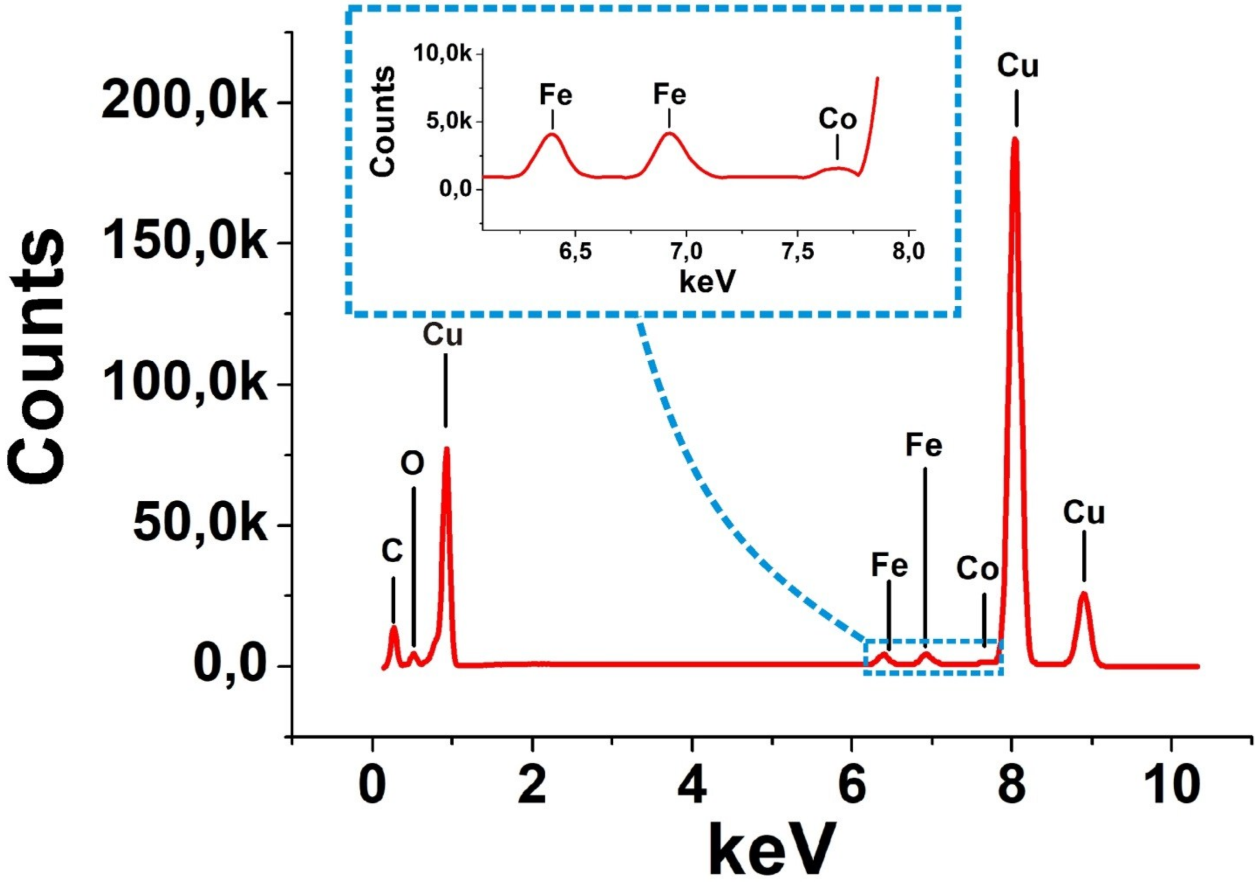

Figure S19 EDS spectrum of **2**. A suspension of the complex **2** was applied to a special substrate for TEM - a copper mesh coated with formvar and carbon. This explains the presence of copper lines in the spectrum. In the spectrum, against the background of intense copper lines, the cobalt line $K_{\beta1} = 7.65$ keV is visible, and we can also state the presence of the cobalt line $L_{\alpha1} = 0.78$ keV, which overlapped the left wing of the copper line $L_{\alpha1} = 0.93$ keV. In addition to cobalt lines, the spectrum contains iron lines ($K_{\alpha1} = 6.41$ keV, $L_{\beta1} = 7.06$ keV), a carbon line ($K_{\alpha1} = 0.28$ keV), an oxygen line ($K_{\alpha1} = 0.53$ keV), and copper lines ($L_{\alpha1} = 0.93$ keV, $K_{\alpha1} = 8.05$ keV, $K_{\beta1} = 8.90$ keV).

```
Sample   : SR53A
Operator:
Comment  : sample cell 5um polypropylene
Group    : powder_air_XXX_PP_He
Date     : 2020-01-20 15:08:06

Measurement Condition
----------------------------------------------------------------------------------
Instrument: 800HS2   Atmosphere: He     Collimator:  5(mm)   Spin: Off
----------------------------------------------------------------------------------
Analyte                 TG kV   uA      FI   Acq.(keV) Anal.(keV)  Time(sec)    DT(%)
----------------------------------------------------------------------------------
Ti-U                    Rh 50   16-Auto ----   0 - 40   0.00-40.00  Live-  99    25
```

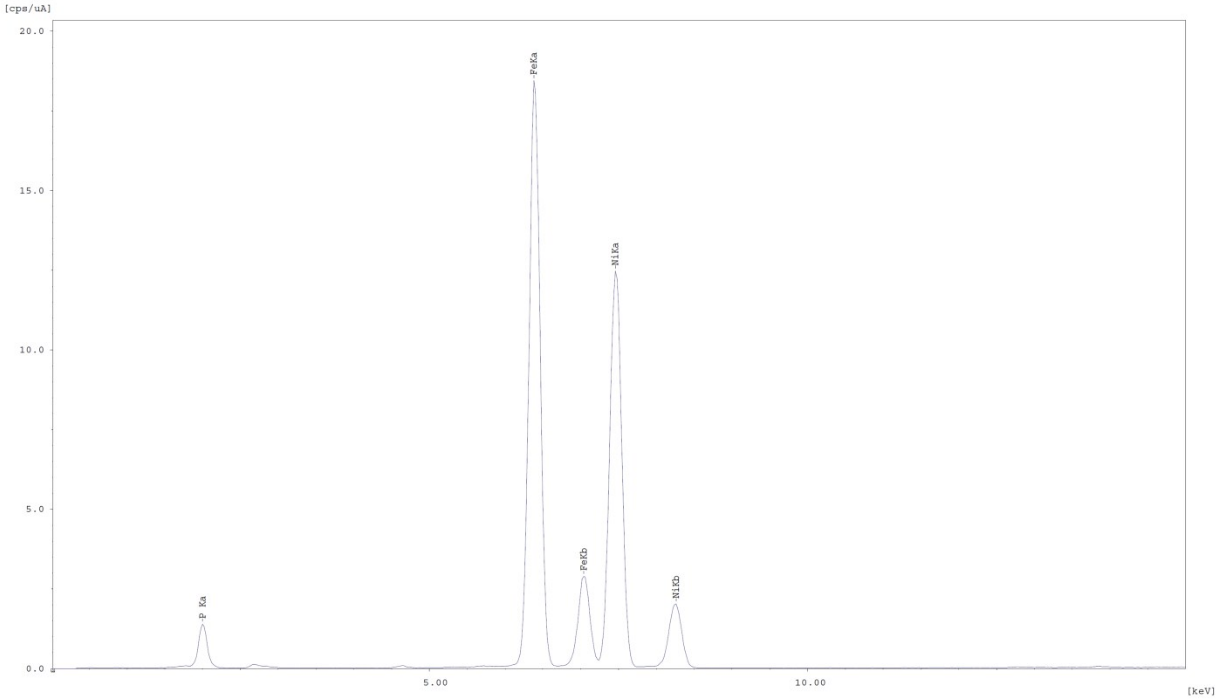

```
Quantitative Result
----------------------------------------------------------------------------------
Analyte                    Result         (Std.Dev.) Proc.-Calc. Line   Int.(cps/uA)
----------------------------------------------------------------------------------
====[No. 1 Layer]====< Layer1              >===================================
                          5.000 um        (------) Fix         -------- --------
CH2                     100.000 %         (------) Fix         -------- --------
====[No. 2 Layer]====< Base                >===================================
Ni                       43.748 %         ( 0.101) Quan-FP     NiKa     117.4727
Fe                       34.350 %         ( 0.068) Quan-FP     FeKa     157.8121
P                        21.901 %         ( 0.088) Quan-FP     P Ka       4.9222
```

Figure S20 X-ray fluorescence analysis of **1**.

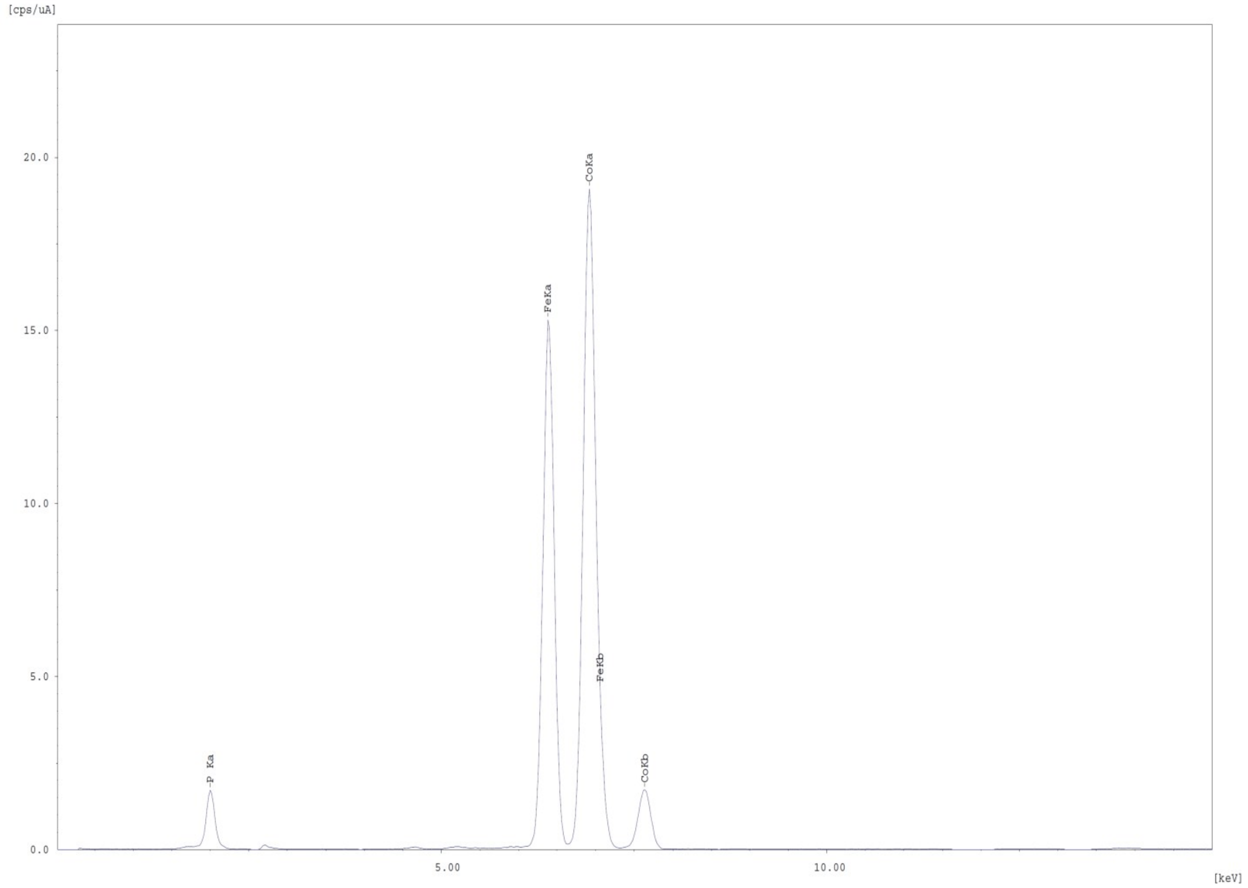

```
Quantitative Result
---------------------------------------------------------------------------------
Analyte                   Result          (Std.Dev.) Proc.-Calc. Line   Int.(cps/uA)
---------------------------------------------------------------------------------
====[No. 1 Layer]====< Layer1               >====================================
                           5.000 um       (------) Fix          -------- --------
CH2                      100.000 %        (------) Fix          -------- --------
====[No. 2 Layer]====< Base                 >====================================
Co                        38.279 %        ( 0.082) Quan-FP      CoKa     158.4673
Fe                        35.575 %        ( 0.077) Quan-FP      FeKa     130.5115
P                         26.146 %        ( 0.101) Quan-FP      P Ka       6.0965
```

Figure S21 X-ray fluorescence analysis of **2**.

References

1. Cao, C. Y.; Wei, K. J.; Ni, J.; Liu, Y., Solvent-induced two heterometallic coordination polymers based on a flexible ferrocenyl ligand. *Inorg. Chem. Comm*. **2010**, *13*, 19-21.
2. Kondo, M., Yoshitomi, T., Matsuzaka, H., Kitagawa, S., & Seki, K. Three-Dimensional Framework with Channeling Cavities for Small Molecules:{[M2(4,4′-bpy)3 (NO3)4]• xH2O}n (M= Co, Ni, Zn). *Angew. Chem. Intern. Ed*., 1997, 36(16), 1725-1727.
3. U. Mueller, N. Darowski, M. R. Fuchs, R. Förster, M. Hellmig, K. S. Paithankar ,S. Pühringer, M. Steffien, G. Zocher and M. S. Weiss, *J. Synchrotron Radiat.* 2012, **19**, 442.
4. M. Krug, M. S. Weiss, U. Heinemann and U. Mueller, *J. Appl. Crystallogr.,* 2012, **45**, 568.
5. G.M. Sheldrick *Acta Cryst.,* 2015, **C71**, 3–8
6. P.-Q. Liao, J.-Q. Shen, J.-P. Zhang, *Coord. Chem. Rev*., **2018**, 373, 22–48
7. M.L. Helm, M.P. Stewart, R.M. Bullock, M.R. DuBois, D.L. DuBois, *Science*, **2011**, 333, 863-866.